Optimizing Robot-Assisted Surgery Suture Plans to Avoid Joint Limits and Singularities

Brijen Thananjeyan[1], Ajay Tanwani[1], Jessica Ji,[1], Danyal Fer[2], Vatsal Patel[1], Sanjay Krishnan[3], Ken Goldberg[1]

***Abstract*—Laparoscopic robots such as the da Vinci Research Kit encounter joint limits and singularities during procedures, leading to errors and prolonged operating times. We propose the Circle Suture Placement Problem to optimize the location and direction of four evenly-spaced stay sutures on surgical mesh for robot-assisted hernia surgery. We present an algorithm for this problem that runs in 0.4 seconds on a desktop equipped with commodity hardware. Simulated results integrating data from expert surgeon demonstrations suggest that optimizing over both suture position and direction increases dexterity reward by 11%-57% over baseline algorithms that optimize over either suture position or direction only.**

I. Introduction

Limited autonomy has been studied for robotic surgical procedures and has the potential to reduce surgeon fatigue, improve precision, and facilitate long-range tele-operation [1–6]. We investigate suture placement planning to avoid joint limits and singularities for robot-assisted hernia surgery on the da Vinci Research Kit (dVRK) [7].

Robot-assisted hernia surgery, in which a surgical mesh is placed over an abdominal wall defect using a robot, is increasingly common and particularly challenging to perform [8]. The success of the repair depends on the mesh being placed tightly enough to restrain the protrusion but loosely enough to ensure healing. The challenging aspect of the procedure is using an articulated robotic wrist, without haptic feedback, to perform a number of precision suturing motions: a set of "stay sutures" are placed to ensure the mesh remains flat and then a running suture to place the mesh. We assume stay sutures are performed on a circle centered on the protrusion in a direction tangent to its boundary. Suturing motions constrained by joint limits and singularities can result in errors and are difficult to predict by a human or semi-autonomous controller before execution of a suture. This limits the ability of the robot to avoid these configurations during needle insertion, which can prevent the needle from following the desired trajectory. In this paper, we explore how the positions and directions of sutures can be optimally planned to avoid areas of the configuration space that are close to joint limits and singularities.

Prior work on autonomous suturing uses self-righting needle fixtures to maintain a consistent and known needle pose during autonomous needle insertion, so we assume the pose of the needle relative to the gripper is fixed [1, 5]. Simulated experiments suggest that optimizing over suture position and direction enables the robot to avoid motions constrained by joint limits and singularities.

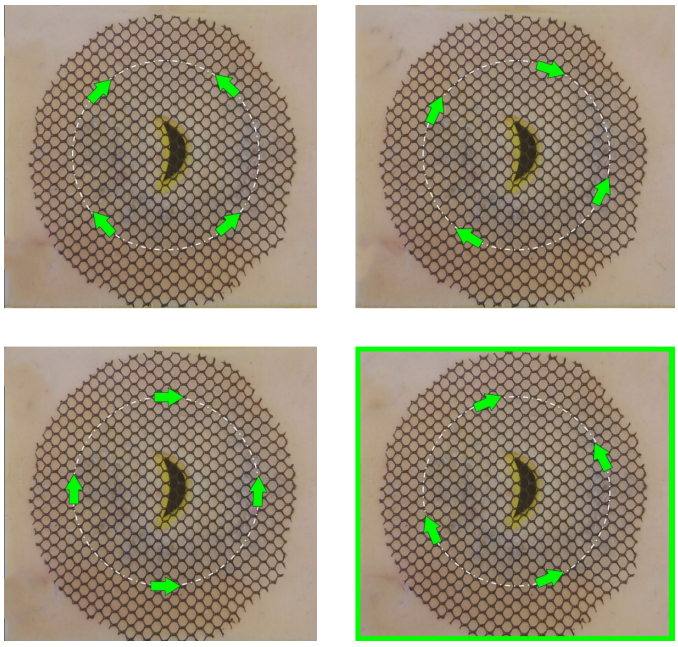

Figure 1: The Circle Suture Plan Optimizer outputs position and orientation for suture throws on the boundary of a given circle with fixed radius centered around the herniated tissue with respect to a dexterity reward defined in Section III-D3 that penalizes motions that are close to joint limits and singularities. The suturing arm is mounted below and to the left of the tissue phantom. We display the optimal directions for evenly-spaced sutures with different initial suture locations and observe that the direction varies in different locations on the phantom. The bottom right image depicts the sequence of sutures that maximizes a weighted combination of joint margin and manipulability rewards by optimizing both suture positions and directions.

In data collected from an expert surgeon on training tissue phantoms obtained from Intuitive Surgical, we observe that the robot encounters variation in manipulability and configurations near joint singularities during placement of the sutures, resulting in unpredictable motions and errors during teleoperation. A dataset containing kinematic data for 16 physically-performed sutures is used to estimate a reward function for sutures that avoid joint singularities. We compare the ability of an algorithm that optimizes both position and direction of evenly-spaced sutures to avoid joint limits and singularities to baseline alternatives that optimize either position or direction only in simulated experiments. Results suggest that optimizing both the position and direction of evenly spaced sutures perform

Authors are affiliated with:
[1]AUTOLAB at UC Berkeley; @berkeley.edu
[2]UC San Francisco East Bay; @ucsf.edu
[3]University of Chicago; @cs.chicago.edu
{bthananjeyan, ajay.tanwani, jji, danyal.fer, vatsal.patel, goldberg}

978-1-5386-7825-1/19/$31.00 ©2019 IEEE

better than optimizing for position or direction alone.

This paper makes three contributions:

1) Proposes the Circle Suture Placement Problem to avoid low-dexterity configurations during robot-assisted hernia repair.
2) Presents an algorithm for the Circle Suture Placement Problem that samples evenly over the set of feasible sequences of sutures. A Python implementation of the algorithm takes 0.4 seconds to run on an Ubuntu PC.
3) Evaluates the algorithm on a simulated setup against baselines that picks random evenly-spaced sutures and baselines that consider sutures in only one direction. The algorithm achieves a dexterity reward $11-57\%$ greater than baselines.

II. Related Work

A. Autonomy in Robotic Surgery and Telesurgery

Robot-assisted surgical platforms improve the field of view and maneuverability for surgeons completing laparoscopic hernia repair. Shraga et al. examine the advancements of this relatively new technique for hernia repair [9]. Bosi et al. present the technical details for and evaluate the efficacy of robot-assisted single site bilateral hernia repair using continuous suture [10]. These works do not consider the improvements in dexterity and ergonomics for surgeons during robot-assisted hernia repair that can be realized through suture placement optimization.

Clinical systems use varying degrees of autonomy, from direct control with the da Vinci Surgical System to supervised autonomy with the CyberKnife system, which precomputes a treatment plan and helps surgeons track moving tumors to deliver radiotherapy [11]. The ROBODOC system performs the femoral preparation step of knee arthoplasty autonomously after a surgeon guided registration sequence [12].

While no minimally invasive supervised autonomy surgical system is used in clinical practice, in the lab setting there has been work done on automating surgical subtasks and primitives such as suturing [1, 5, 13–16], cutting [2], steerable needle guidance [17], prob alignment [18], grasping [19], debridement [20, 21], and tensioning [22]. D'Etorre et al. designed a system that performs closed-loop visual servoing with the assistance of a surgeon to complete the needle handoff step in suturing [14]. Jackson et al. and Russell et al. formulated and evaluated a motion planning procedure to analytically generate robot trajectories to perform suture throws without visual feedback [15, 23]. We define a similar needle insertion motion.

Shademan et al. designed the Smart Tissue Autonomous Robot (STAR) to perform supervised autonomous anastomosis with near-infrared fluorescent (NIRF) imaging to track tissue motion [5]. They demonstrate that their system, built with a 7-DOF Kuka LWR 4+ industrial arm and a 1-DOF Endo360 suturing tool, outperformed human and robot-assisted human surgeons in leak pressure and suture spacing.

B. Dexterity Optimization and Human-Robot Collaboration

Within the problem subspace of dexterity optimization [24], many metrics have been proposed for characterizing the dexterity and performance of robot arms [25]. The spatial Jacobian $J(q) \in \mathbb{R}^{m \times n}$ of the robot is widely used to assess the end-effector velocities $\dot{x} \in \mathbb{R}^m$ that can be generated by input joint velocities $\dot{q} \in \mathbb{R}^n$ with $\dot{x} = J(q)\,\dot{q}$ [26]. This defines a *manipulability ellipsoid* and its properties can be summarized through functions related to its semi-axis lengths (the singular values σ of $J(q)$) [27, 28]. The Euclidean norm of $\|\dot{q}\| \leq 1$ or $\dot{x}^T(JJ^T)^{-1}\dot{x} \leq 1$ defines an ellipsoid. The end-effector can move at high speed along the principal axis of this ellipsoid, but can only move at a very low speed along the minor axis. Related dexterity metrics include the manipulability index, the condition number, and the parameter of singularity. Zargarbashi et al. use condition number as a performance index to improve joint-rate distribution [29]. Another strategy is to avoid joint limits of the robot, which are not necessarily encoded by information in the robot Jacobian. Huo et al. propose a joint cost between singularity and joint limit avoidance for the task of robotic welding [30]. Garg et al. study needle path planning in the presence of occluded volumes for automated brachytherapy [31]. We propose a similar problem to avoid constrained regions for semi-autonomous suturing on surgical mesh.

Within robot learning, prior work investigates algorithms that allow robots to learn from human interaction through measurements such as physical corrections and disturbances [32, 33] as well as EEG-measured error-related potentials from a human operator [34]. Human-robot collaboration has also been well studied. Edsinger et al. demonstrate that in response to reaching gestures, human subjects can successfully hand objects to and take objects from a robot [35]. It is important to note that in human-robot control transfer, the final pose of the object affects the subject's ability to grasp [36]. Several papers present frameworks for producing safe, ergonomic human-robot interaction by generating robot motions via cost functions that optimize subject safety, posture, vision field, and kinematics [37, 38]. Other metrics have been created to measure performance during human interaction [39].

III. Circle Suture Placement Problem

A. Overview

The surgeon inputs the center and radius of a circle to the Circle Suture Placement Planner, which plans an optimal sequence of suture positions and directions. In this paper, we investigate the effect of modifying the location and direction of sutures.

The optimal location and direction of four evenly-spaced sutures are computed by solving the Circle Suture Placement Algorithm outlined in this section.

B. Notation

A position on a given circle is identified by the single angle θ_i. Direction d_i of a suture on the boundary of a circle is clockwise if $d_i = +1$ and counterclockwise if $d_i = -1$. The placement of suture i on a given circle can be identified by a tuple (θ_i, d_i)

where $\theta_i \in [0, 2\pi)$ and $d_i \in \{-1, +1\}$. Unless otherwise specified, the best direction d_i is selected, so the suture is referred to by its position θ_i in the remainder of the paper. The procedure to select the best direction is discussed Section III-D1. A sequence of four evenly spaced sutures is called a *suture plan* and is represented by $(\theta_1, d_1), (\theta_2, d_2), (\theta_3, d_3), (\theta_4, d_4)$. Because the best direction at a position is selected unless otherwise specified, the location of the first suture uniquely specifies the entire suture plan. We identify suture plans by their first suture position θ_1.

C. Assumptions

1) Suture Placement: We assume that evenly-spaced sutures are required to maintain tension in the surgical mesh. Sutures are constrained to be placed tangent to the boundary of a circle on the tissue phantom specified by the surgeon. Sutures can be thrown either clockwise or counterclockwise on the circle, but must be thrown in a direction tangent to the circle. We assume permuting the order of the stay sutures does not affect the configurations encountered when performing the task. The phantom is at a fixed, known position centered in the workspace of the arms.

2) Needle Insertion: To construct robot trajectories for autonomous needle insertion for evaluation in simulated analysis, we define a motion primitive to perform this task. The motion is hand-tuned to maximally avoid joint limits when multiple feasible trajectories exist to perform the same suture, but the same end-effector is used for needle insertion at all areas of the workspace. This restriction is imposed because prior work on autonomous suturing uses fixtures to stabilize the needle pose during the needle insertion motion [1, 5]. We assume that the pose of the needle relative to the grippers is a known constant and that the surgeon is able to load the needle into the gripper in between sutures to accomplish this. The specific parameters assumed for this motion are discussed in Section IV-A1. An implementation of the motion is not physically evaluated in experiments, and all semi-autonomous analyses are conducted in simulation. The experiments consider a setup with two 7-DOF dVRK arms with a fixed Remote Center of Motion (RCM).

3) Reward Function: We assume that only the wrist joints are constrained, because the remaining joints are far from joint limits during the task. However, the approach in this paper is extensible to all robot joints in tasks where non-wrist joints are also constrained. We weight all wrist joints and arms evenly and assume that the start and end poses of a needle insertion provide a sufficiently accurate bound for the wrist joint angles during suturing. We are also limited by the set of 16 physical demonstrations collected to estimate the distribution of joint states visited by the surgeon during teleoperation. This distribution is used to estimate the average manipulability index. The distributions used to define the reward in Section III-D2 can vary across surgeons and across circle positions.

D. Dexterity Reward

1) Joint Margin: The needle insertion planner described in Section IV-A1 and Figure 2 fails to guide the needle in the defined trajectory when the desired wrist joint configuration of the arm approaches or exceeds joint limits q_{limit}. The wrist joint angles are centered around 0, and to penalize needle insertion motions that are close to joint limits, we compute the maximum absolute joint angle for each wrist joint over the desired start and end poses of the needle insertion arm during needle insertion. We compute this in both directions at θ_i on the circle by computing the inverse kinematics of a simulated da Vinci arm. We let $q_{max,d}(\theta_i)$ denote the vector containing the maximum absolute joint angles for the needle insertion at θ_i in direction d.

The nonnegative *joint margin* is defined to be $Q(\theta_i) = \max_{d \in \{-1,+1\}} \| |q_{max,d}(\theta_i)| - q_{limit} \|_2^2$. This function quadratically rewards configurations that avoid joint limits for the best suture direction at θ_i. Q maps a position to a nonnegative real number and is used to select the optimal direction of a suture.

2) Manipulability Reward: The *squared manipulability index* of a joint configuration q of a robot arm with Jacobian J is defined as $|J(q)J(q)^T|$. This function indicates the range of twists t that can be generated at q and has been used to optimize base placement of the da Vinci Research Kit to avoid regions near joint singularities [40]. We observe that manipulability varies during teleoperated needle extraction and thread manipulation, which is associated with unpredictable motions of the robot arms and errors (Figure 6).

Therefore, we define a nonnegative *manipulability reward* $M(\theta_i) = \mathbb{E}_{\theta_i} |J(q)J(q)^T|$ which evaluates the average squared manipulability index where $\mathbb{E}_{\theta_i}$ indicates expectation with respect to the distribution of joint configurations visited when performing a suture at θ_i. Both arms are considered equally for this reward, which maps a position to a nonnegative real number. We discuss how this function is approximated in Section IV-A2 and its variability in Section IV-C.

3) Dexterity Reward: The optimization problem considered in Section III-H considers a weighted combination of the joint margin and manipulability reward. The *dexterity reward* $D(\theta) = \min_{1 \le i \le 4} \lambda Q(\theta_i) + (1 - \lambda) M(\theta_i)$. The parameter λ weights Q and M where $\lambda \in [0, 1]$. The dexterity reward reports the value for the lowest scoring suture. Both functions are adjusted to occupy the same range before relatively weighting each reward with λ. We numerically evaluate the sensitivity of this parameter in Section IV-D. We use $\lambda = 0.75$, because the optimal plan at this setting is robust to variation in λ (Figure 7).

4) Integral Positions: To solve for the optimal suture plan, the set of all possible positions is approximated by $[0, 360) \cap \mathbb{Z}$, which restricts suture positions to integral values.

E. Input

The surgeon provides the parameters for a circle centered on the hernia phantom as input.

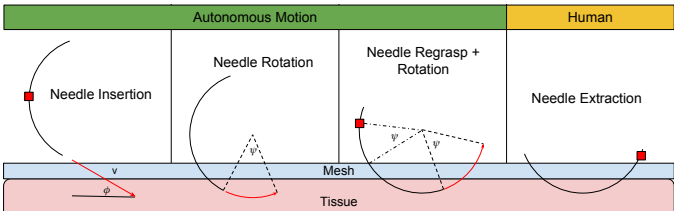

Figure 2: To evaluate the joint margin Q, we divide a suture into a sequence of semantically significant steps. (1) The needle penetrates the tissue phantom in a straight path of length $v = 1.0$ cm at a fixed entry angle $\phi = 30^\circ$. (2) The needle is rotated $\psi = 70^\circ$ to follow a path generated by its curvature. (3) The needle is then regrasped further up and rotated a fixed number of times. (4) Finally, the surgeon manually pulls out the needle and thread and prepares for the next suture. The red squares indicate needle grasps by the needle insertion arm. The start and end joint angles of the first three steps are used to evaluate q_{max}, which is used to evaluate the joint margin and best suture direction. This reference trajectory is similar to the one implemented by Jackson et al. [15].

F. Output

The algorithm outputs an optimal suture plan that maximizes the minimum weighted sum of joint margin and manipulability reward over all sutures.

G. Circle Suture Placement Problem

Under these assumptions, finding an optimal sequence of sutures is equivalent to solving the following *Circle Suture Placement Problem*:

$$\theta^* = \arg\max_{\theta} \min_{1 \le i \le 4} \lambda Q(\theta_i) + (1-\lambda) M(\theta_i)$$

such that

$$\theta_{(i+1) \bmod 4} - \theta_i = 90 \ \forall i \in \{1,2,3,4\} \text{ (evenly-spaced sutures)}$$

$$\theta_i \in \mathbb{Z} \cap [0, 360) \ \forall i \in \{1,2,3,4\} \text{ (integral angles)}$$

The solution to this problem maximizes the distance to joint limits and average manipulability when performing a sequence of evenly-spaced semi-autonomous sutures. The two constraints force the resulting suture locations to be evenly-spaced and placed at integral locations on the boundary of the circle. The first constraint also fixes the ordering of the vector θ that contains the locations of the sutures. The direction of each suture is chosen by selecting the direction with greatest joint margin for each θ_i^*.

H. Circle Suture Placement Algorithm

The solution space of the problem includes $90 * 2^4 = 1440$ feasible plans, and we find that exhaustive search is tractable and effective under the assumptions stated in this paper. A single-threaded Python implementation of this algorithm computes a solution in 0.4 seconds on an Ubuntu PC with commodity hardware.

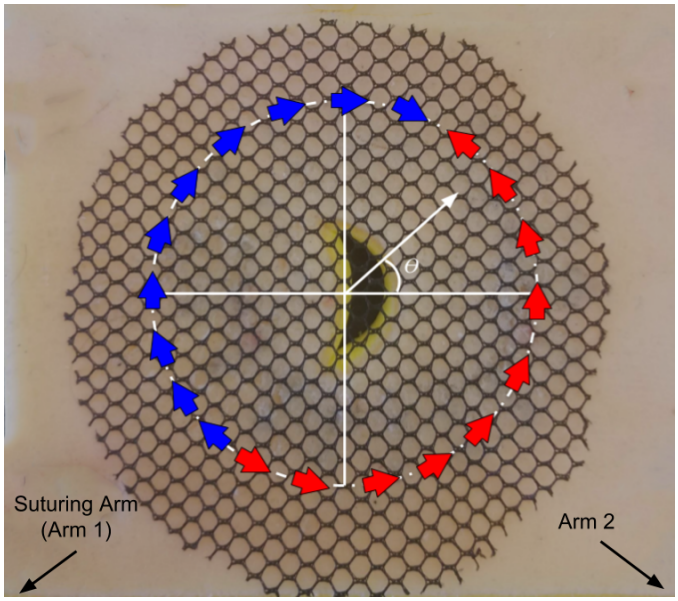

Figure 3: The optimal suture direction changes as a function of position on the circle. The suturing arm originates at a point below and to the left of the tissue phantom. The changes in suture direction correspond to discontinuities in the joint state in Figure 4 and points where joint margins in either direction are equal in Figure 5.

IV. Experimental Setup and Simulated Results

A. Reward Function Evaluation

1) Joint Margin: The open-loop controller discussed in Figure 2 is used to evaluate the joint margin a priori during suture plan optimization. The needle insertion primitive takes in a position and a heading and performs an initial needle penetration and rotation in the phantom followed by 2 motions to push the needle further through the phantom after regrasping. The nominal trajectories for insertions on the circle are tuned to compensate for kinematic inaccuracies of the robot. Although the pose of the needle relative to the gripper is fixed, we observe this restriction does not affect the existence of high joint margin sutures at positions on the circle (Figure 5).

2) Manipulability Reward: Because surgeon maneuvers are difficult to model, to evaluate M in practice, we record kinematic data for two physical demonstrations of fully-teleoperated sutures at eight evenly-spaced locations on the circle. This data is used to approximate the distribution of joint configurations encountered when suturing at these points. Due to kinematic and system constraints, we allow the surgeon to select the preferred direction for needle insertion.

At the positions used in the demonstrations, M is estimated exactly by computing the mean-squared manipulability index across both robot arms in the corresponding demonstrations. To evaluate M at positions that are not in the demonstration set, we linearly interpolate M between the two closest positions in the demonstrations.

B. Joint Angle Analysis

We compute and plot $\min_{d \in \{-1,+1\}} q_{max,d}(\theta_i)$ as a function of θ_i in Figure 4 and observe the existence of regimes where joint range availability is limited. We observe that the needle

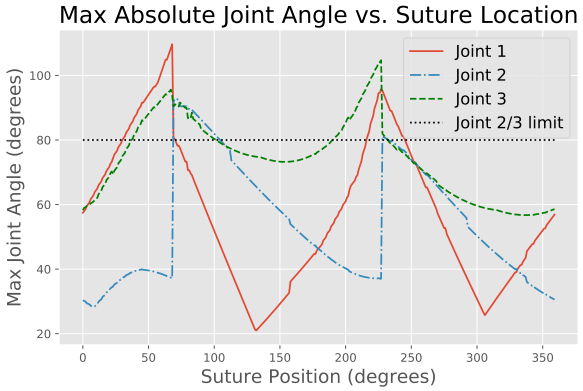

Figure 4: The maximum wrist angles $\min_{d\in\{-1,+1\}} q_{max,d}(\theta_i)$ of the suturing arm during autonomous needle insertion is a function of the location on the circle. Joint 1 has range $[-260,260]$ and joint 2 and joint 3 have range $[-80,80]$. Safe regions that maintain a distance to the joint limits occur near the sets $[0,30],[140,160]$, and $[300,360)$ and large jumps at 67° and 228° indicate points where the optimal direction changes. The black, dashed line indicates joint limits for two of the wrist joints.

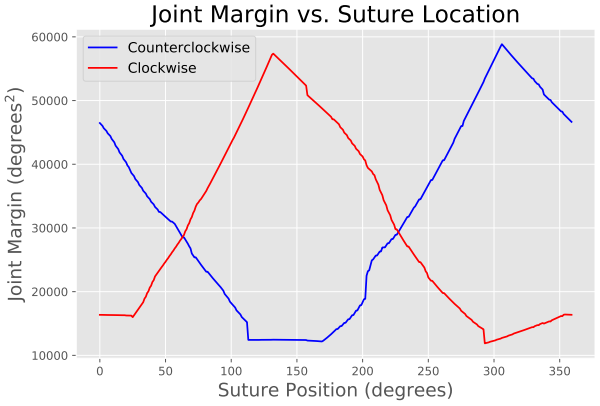

Figure 5: The joint margin is evaluated for sutures placed on the boundary of the circle. We observe this value is high in at least one direction at all positions and the transition points between preferred arms occur at $\theta = 67°$ and $\theta = 228°$.

insertion primitive can still guide the needle in a feasible trajectory at locations where joint 3 saturates if it is close to the desired pose.

We also plot the joint margin for all sutures in either direction as a function of start angle (Figure 5). The analysis suggests that joint margin can be increased significantly by selecting suture direction optimally. Sutures with low joint margin can be avoided by performing the suture in the opposite direction. Solving for the direction that maximizes joint margin, Figure 3 plots the optimal direction for sutures on the circle.

C. Manipulability Analysis

We collect two physical demonstrations at 8 evenly-spaced points and plot the manipulability reward M of the robot's arms at each point in Figure 6. We observe that regions with high manipulability for one arm correspond to regions with low manipulability for the other arm. For example, the first arm

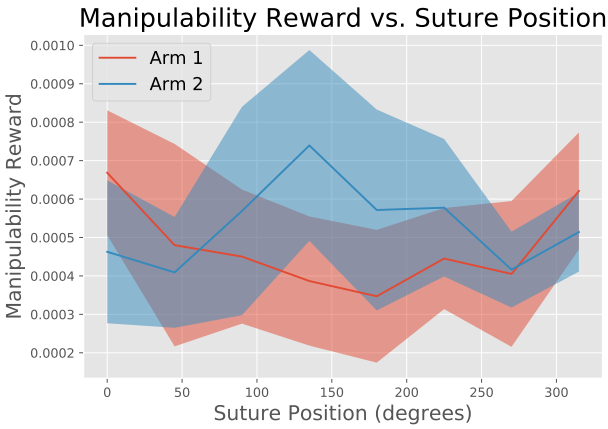

Figure 6: Manipulability reward M is displayed as a function of the suture location on the circle for physically performed suture throws. Arm 1 is used to insert the needle into the phantom, and Arm 2 is used to extract the needle and prepare Arm 1 for the next suture. We observe variance in manipulability and regions on the circle where the robot has lower manipulability on average. We observe that the individual arms have complementary regions of high manipulability.

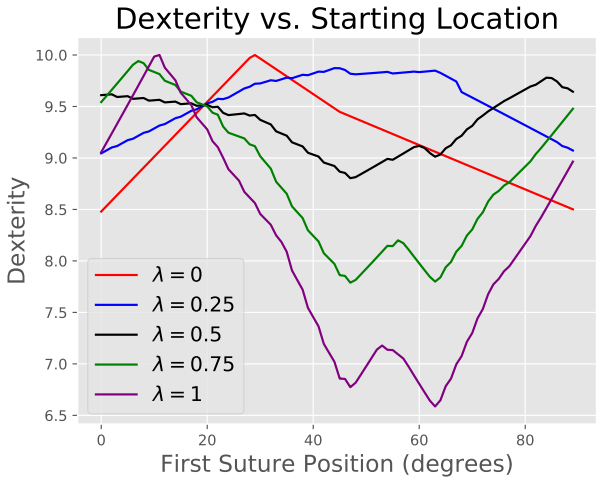

Figure 7: Sensitivity to different values of λ. The individual reward functions are scaled such that each function has maximum value 10 when maximum weight is placed on it before reweighting with λ. Increasing λ increases the weight for the joint margin, and this decreases the reward for plans that get close to joint limits. The maximizer of each function is sensitive to the choice of λ. Plans that start with $\theta_1 \in [40,80]$ are particularly sensitive to λ as a result and increasing λ moves the optimal starting location from 28° to 11°. The range $[40,80]$ corresponds to the region in Figure 5 where both arms have relatively low joint margin, so increasing the weight on the joint margin drastically reduces the dexterity.

has high manipulability during sutures performed at positions near $[100,250]$ while the second has low manipulability in this region. The converse is true in the region $[0,50]\cup[300,360)$. We hypothesize that this is explainable by the symmetry of the positioning of the arms relative to the tissue phantom, which is centered in the workspace, and that points closer to the base of the arm appear to experience lower average manipulability.

D. Weighting Factor Sensitivity Analysis

In this experiment, the graph of the dexterity reward is plotted for several values of λ (Figure 7). We observe that increasing λ moves the the optimal plan from $\theta_1 = 28^\circ$ to $\theta_1 = 11^\circ$. Increasing λ also penalizes plans where θ_1 is in the range $[40, 80]$, because these plans have low joint margins. We use $\lambda = 0.75$ in the remaining experiments, because the variance in the dexterity of the optimal plan for this setting is small across different values of λ.

E. Comparison to Baselines

In Table I, we numerically evaluate the dexterity reward of performing this optimization procedure against a set of baselines. Each baseline is defined by two components: a selection method for the first suture position and a selected suture direction. Sutures can be performed clockwise, counterclockwise, or in the optimal direction. The expected reward for randomized methods is computed exactly by averaging over all possible suture plans. The rewards are scaled such that the best algorithm of any of the baselines is given a score of 100. To further elaborate, the set of baselines considered are:

1) **Random Location, Clockwise Direction**: Uniformly at random selects a location for the starting suture and only allows sutures performed in a clockwise manner.
2) **Random Location, Counterclockwise Direction**: Uniformly at random selects a location for the starting suture and only allows sutures performed in a counterclockwise manner.
3) **Random Location, Optimal Direction**: Uniformly at random selects a location for the starting suture and optimizes over the direction of the suture as well.
4) **Optimal Location, Clockwise Direction**: Optimizes over the locations of the sutures with respect to dexterity with only clockwise sutures.
5) **Optimal Location, Counterclockwise Direction**: Optimizes over the locations of the sutures with respect to dexterity with only counterclockwise sutures.

We observe in Table I that optimizing over both direction and position of the sutures yields a dexterity reward 11-57% higher than baselines that optimized over either position or direction only. Optimizing direction provides a larger performance gain than optimizing location, because the needle throw motion was constructed in such a manner that at least one direction at a given position has high dexterity as noted in Figure 5.

Table I: **Dexterity Improvement of Circle Suture Placement Planning vs. Baselines:** In this table, the reward of optimizing both position and direction is compared against baselines that optimize over position or direction only. The results indicate that optimizing both position and direction of the sutures increases dexterity reward 11.4% over the next best algorithm and 57.2% over the best algorithm that sutures in a fixed direction. Optimizing the direction alone provides a large performance gain relative to fixing a direction. This occurs because certain regions that are difficult for sutures in a particular direction are unavoidable, but the set of positions that have low dexterity for either direction are approximately complementary.

Location Selection	**Allowable Directions**		
	Clockwise	***Counterclockwise***	***Optimal***
Random	60.2	42.8	88.6
Optimal	**65.6**	**50.6**	**100.0**

V. Future work

In future work, we will explore how mesh tension properties would allow for relaxation of optimization constraints such as number of sutures and suture consistency and how modifying the center and radius of the circle would affect dexterity. The relaxation of these parameters increases the dimensionality of the feasible set of sequences, so we plan to explore how binary search and derivative-free numerical optimization can be used to solve dexterity optimization problems when the set of task plans is large and discretization is ineffective. We will physically evaluate the mesh tension and arm performance for optimal and suboptimal suture plans. With a larger set of surgeon data, the distribution of joint states visited during a suture can be more accurately estimated, enabling better planning. Another exciting area of future research is characterizing the contribution of each joint to errors and weighting each joint proportionally in the construction of the joint margin and manipulability reward.

Acknowledgment

This research was performed at the AUTOLAB at UC Berkeley in affiliation with BAIR and the CITRIS "People and Robots" (CPAR) Initiative: http://robotics.citris-uc.org in affiliation with UC Berkeley's Center for Automation and Learning for Medical Robotics (Cal-MR). The authors were supported in part by donations and a major equipment grant from Intuitive Surgical. We thank Daniel Seita for his extensive feedback on this manuscript.

References

[1] S. Sen, A. Garg, D. V. Gealy, S. McKinley, Y. Jen, and K. Goldberg, "Automating Multiple-Throw Multilateral Surgical Suturing with a Mechanical Needle Guide and Sequential Convex Optimization", in *ICRA*, 2016 (cit. on pp. 1–3).

[2] A. Murali, S. Sen, B. Kehoe, A. Garg, S. McFarland, S. Patil, W. D. Boyd, S. Lim, P. Abbeel, and K. Goldberg, "Learning by observation for surgical subtasks: Multilateral cutting of 3d viscoelastic and 2d orthotropic tissue phantoms", in *ICRA*, IEEE, 2015, pp. 1202–1209 (cit. on pp. 1, 2).

[3] J. Schulman, A. Gupta, S. Venkatesan, M. Tayson-Frederick, and P. Abbeel, "A Case Study of Trajectory Transfer through Non-Rigid Registration for a Simplified Suturing Scenario", in *IROS*, 2013, pp. 4111–4117 (cit. on p. 1).

[4] M. Yip and N. Das, "Robot autonomy for surgery", *CoRR*, vol. abs/1707.03080, 2017. arXiv: 1707.03080 (cit. on p. 1).

[5] A. Shademan, R. S. Decker, J. D. Opfermann, S. Leonard, A. Krieger, and P. C. Kim, "Supervised autonomous robotic soft tissue surgery", *Science translational medicine*, vol. 8, no. 337, 337ra64–337ra64, 2016 (cit. on pp. 1–3).

[6] A. K. Tanwani and S. Calinon, "A generative model for intention recognition and manipulation assistance in teleoperation", in *IEEE/RSJ International Conference on Intelligent Robots and Systems, IROS*, 2017, pp. 43–50 (cit. on p. 1).

[7] P. Kazanzides, Z. Chen, A. Deguet, G. S. Fischer, R. H. Taylor, and S. P. DiMaio, "An open-source research kit for the da vinci surgical system", in *IEEE Intl. Conf. on Robotics and Auto. (ICRA)*, Hong Kong, China, Jun. 1, 2014, pp. 6434–6439 (cit. on p. 1).

[8] M. Nguyen, R. Berger, S. Hicks, J. Davila, K. Li, L. Kao, and M. Liang, "Comparison of outcomes of synthetic mesh vs suture repair of elective primary ventral herniorrhaphy: A systematic review and meta-analysis", *JAMA Surgery*, vol. 149, no. 5, pp. 415–421, 2014. eprint: /data/journals/surg/930220/soi130131.pdf (cit. on p. 1).

[9] D. R. Sarrina Shraga Erin Chang and G. Sugiyama, "Chapter 3 robotic inguinal hernia repair", 2017 (cit. on p. 2).

[10] H. R. Bosi, J. R. Guimarães, and L. T. Cavazzola, "Robotic assisted single site for bilateral inguinal hernia repair", in *Arquivos brasileiros de cirurgia digestiva : ABCD = Brazilian archives of digestive surgery*, 2016 (cit. on p. 2).

[11] S. Dieterich and I. Gibbs, "The cyberknife in clinical use: Current roles, future expectations", vol. 43, pp. 181–94, May 2011 (cit. on p. 2).

[12] E. H. Spencer, "The robodoc clinical trial: A robotic assistant for total hip arthroplasty", vol. 15(1), pp. 9–14, 1996 (cit. on p. 2).

[13] F. Nageotte, P. Zanne, C. Doignon, and M. de Mathelin, "Stitching planning in laparoscopic surgery: Towards robot-assisted suturing", *The International Journal of Robotics Research*, vol. 28, no. 10, pp. 1303–1321, 2009. eprint: https://doi.org/10.1177/0278364909101786 (cit. on p. 2).

[14] C. D'Ettorre, G. Dwyer, X. Du, F. Chadebecq, F. Vasconcelos, E. D. Momi, and D. Stoyanov, "Automated pick-up of suturing needles for robotic surgical assistance", *CoRR*, vol. abs/1804.03141, 2018. arXiv: 1804.03141 (cit. on p. 2).

[15] R. C. Jackson and M. C. Cavusoglu, "Needle path planning for autonomous robotic surgical suturing", *2013 IEEE International Conference on Robotics and Automation*, pp. 1669–1675, 2013 (cit. on pp. 2, 4).

[16] J. van den Berg, S. Miller, D. Duckworth, H. Hu, A. Wan, X. Fu, K. Goldberg, and P. Abbeel, "Superhuman performance of surgical tasks by robots using iterative learning from human-guided demonstrations", in *2010 IEEE International Conference on Robotics and Automation*, May 2010, pp. 2074–2081 (cit. on p. 2).

[17] J. van den Berg, S. Patil, R. Alterovitz, P. Abbeel, and K. Goldberg, "Lqg-based planning, sensing, and control of steerable needles", in *wafr*, Dec. 2010 (cit. on p. 2).

[18] R. Roy, W. Chen, L. Cong, L. A. Goodell, D. J. Foran, and J. P. Desai, "A semi-automated positioning system for contact-mode atomic force microscopy (afm)", *IEEE Transactions on Automation Science and Engineering*, vol. 10, pp. 462–465, 2013 (cit. on p. 2).

[19] G. Tholey and J. P. Desai, "A modular, automated laparoscopic grasper with three-dimensional force measurement capability", *Proceedings 2007 IEEE International Conference on Robotics and Automation*, pp. 250–255, 2007 (cit. on p. 2).

[20] D. Seita, S. Krishnan, R. Fox, S. McKinley, J. Canny, and K. Goldberg, "Fast and Reliable Autonomous Surgical Debridement with Cable-Driven Robots Using a Two-Phase Calibration Procedure", in *IEEE International Conference on Robotics and Automation (ICRA)*, 2018 (cit. on p. 2).

[21] B. Kehoe, G. Kahn, J. Mahler, J. Kim, A. Lee, A. Lee, K. Nakagawa, S. Patil, W. D. Boyd, P. Abbeel, and K. Goldberg, "Autonomous multilateral debridement with the raven surgical robot", in *2014 IEEE International Conference on Robotics and Automation (ICRA)*, May 2014, pp. 1432–1439 (cit. on p. 2).

[22] B. Thananjeyan, A. Garg, S. Krishnan, C. Chen, L. Miller, and K. Y. Goldberg, "Multilateral surgical pattern cutting in 2d orthotropic gauze with deep reinforcement learning policies for tensioning", *2017 IEEE International Conference on Robotics and Automation (ICRA)*, pp. 2371–2378, 2017 (cit. on p. 2).

[23] R. C. Jackson and M. C. Çavuşoğlu, "Needle path planning for autonomous robotic surgical suturing", in *2013 IEEE International Conference on Robotics and Automation*, May 2013, pp. 1669–1675 (cit. on p. 2).

[24] K. M. Lynch and F. C. Park, *Modern Robotics: Mechanics, Planning, and Control*. Cambridge University Press, 2017 (cit. on p. 2).

[25] S. Patel and T. Sobh, "Manipulator performance measures - a comprehensive literature survey", *Journal of Intelligent & Robotic Systems*, vol. 77, no. 3, pp. 547–570, Mar. 2015 (cit. on p. 2).

[26] B. Siciliano and O. Khatib, *Springer handbook of robotics*. Springer, 2016 (cit. on p. 2).

[27] T. Yoshikawa, "Translational and rotational manipulability of robotic manipulators", *1990 American Control Conference*, pp. 228–233, 1990 (cit. on p. 2).

[28] S. L. Chiu, "Task compatibility of manipulator postures", *The International Journal of Robotics Research*, vol. 7, no. 5, pp. 13–21, 1988 (cit. on p. 2).

[29] J. A. S.H.H. Zargarbashi Waseem Khan, "The jacobian condition number as a dexterity index in 6r machining robots", in *Robotics and Computer-Integrated Manufacturing*, vol. 28, 2012, pp. 694–699 (cit. on p. 2).

[30] L. Huo and L. Baron, "The joint-limits and singularity avoidance in robotic welding", *Industrial Robot: An International Journal*, vol. 35, no. 5, pp. 456–464, 2008 (cit. on p. 2).

[31] A. Garg, T. Siauw, G. Yang, S. Patil, J. A. M. Cunha, I.-C. Hsu, J. Pouliot, A. Atamtürk, and K. Y. Goldberg, "Exact reachability analysis for planning skew-line needle arrangements for automated brachytherapy", *2014 IEEE International Conference on Automation Science and Engineering (CASE)*, pp. 524–531, 2014 (cit. on p. 2).

[32] A. Bajcsy, D. P. Losey, M. K. O'Malley, and A. D. Dragan, "Learning robot objectives from physical human interaction", in *CoRL*, 2017 (cit. on p. 2).

[33] ——, "Learning from physical human corrections, one feature at a time", in *HRI*, 2018 (cit. on p. 2).

[34] A. F. Salazar-Gomez, J. DelPreto, S. Gil, F. H. Guenther, and D. Rus, "Correcting robot mistakes in real time using eeg signals", *2017 IEEE International Conference on Robotics and Automation (ICRA)*, pp. 6570–6577, 2017 (cit. on p. 2).

[35] A. Edsinger and C. C. Kemp, "Human-robot interaction for cooperative manipulation: Handing objects to one another", *RO-MAN 2007 - The 16th IEEE International Symposium on Robot and Human Interactive Communication*, pp. 1167–1172, 2007 (cit. on p. 2).

[36] A. C. B. Mathias Kölsch and M. Turk, "The postural comfort zone for reaching gestures", in *Proceedings of the Human Factors and Ergonomics Society Annual Meeting*, vol. 47, Oct. 2003, pp. 787–791 (cit. on p. 2).

[37] E. A. Sisbot, L. F. Marin-Urias, X. Broquère, D. Sidobre, and R. Alami, "Synthesizing robot motions adapted to human presence - a planning and control framework for safe and socially acceptable robot motions", *I. J. Social Robotics*, vol. 2, pp. 329–343, 2010 (cit. on p. 2).

[38] B. Busch, G. Maeda, Y. Mollard, M. Demangeat, and M. Lopes, "Postural optimization for an ergonomic human-robot interaction", *2017 IEEE/RSJ International Conference on Intelligent Robots and Systems (IROS)*, pp. 2778–2785, 2017 (cit. on p. 2).

[39] F. Dimeas, V. C. Moulianitis, and N. Aspragathos, "Manipulator performance constraints in human-robot cooperation", *Robotics and Computer-Integrated Manufacturing*, vol. 50, pp. 222–233, 2018 (cit. on p. 2).

[40] I. Papanikolaidi, A. Synodinos, V. Moulianitis, N. Aspragathos, and E. Xidias, "Optimal base placement of the da vinci system based on the manipulability index", International Conference on Intelligent Robots and Systems, Sep. 2013 (cit. on p. 3).